analytical chemistry

pubs.acs.org/ac Article

# α-Cyano-4-hydroxycinnamic Acid and Tri-Potassium Citrate Salt Pre-Coated Silicon Nanopost Array Provides Enhanced Lipid Detection for High Spatial Resolution MALDI Imaging Mass Spectrometry

Martin Dufresne, Jarod A. Fincher, Nathan Heath Patterson, Kevin L. Schey, Jeremy L. Norris, Richard M. Caprioli, and Jeffrey M. Spraggins*

Cite This: *Anal. Chem.* 2021, 93, 12243−12249 Read Online

ACCESS | Metrics & More | Article Recommendations | Supporting Information

**ABSTRACT:** We have developed a pre-coated substrate for matrix-assisted laser desorption/ionization (MALDI) imaging mass spectrometry (IMS) that enables high spatial resolution mapping of both phospholipids and neutral lipid classes in positive ion mode as metal cation adducts. The MALDI substrates are constructed by depositing a layer of α-cyano-4-hydroxycinnamic acid (CHCA) and potassium salts onto silicon nanopost arrays (NAPA) prior to tissue mounting. The matrix/salt pre-coated NAPA substrate significantly enhances all detected lipid signals allowing lipids to be detected at lower laser energies than bare NAPA. The improved sensitivity at lower laser energy enabled ion images to be generated at 10 μm spatial resolution from rat retinal tissue. Optimization of matrix pre-coated NAPA consisted of testing lithium, sodium, and potassium salts along with various matrices to investigate the increased sensitivity toward lipids for MALDI IMS experiments. It was determined that pre-coating NAPA with CHCA and potassium salts before thaw-mounting of tissue resulted in a signal intensity increase of at least 5.8 ± 0.1-fold for phospholipids and 2.0 ± 0.1-fold for neutral lipids compared to bare NAPA. Pre-coating NAPA with matrix and salt also reduced the necessary laser power to achieve desorption/ionization by ∼35%. This reduced the effective diameter of the ablation area from 13 ± 2 μm down to 8 ± 1 μm, enabling high spatial resolution MALDI IMS. Using pre-coated NAPA with CHCA and potassium salts offers a MALDI IMS substrate with broad molecular coverage of lipids in a single polarity that eliminates the need for extensive sample preparation after sectioning.

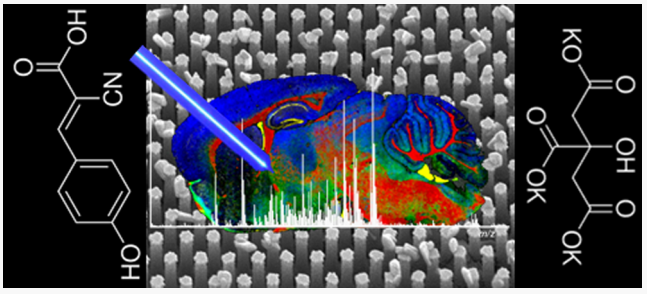


## INTRODUCTION

Imaging mass spectrometry (IMS) enables label-free mapping of endogenous molecules in biological tissues.[1] Various IMS sampling technologies have been developed, with matrix-assisted laser desorption/ionization (MALDI) being the most widely used.[2,3] MALDI has remained at the forefront of IMS due to its capability to generate high spatial resolution images with good sensitivity for a wide variety of biomolecular classes.[4−7] MALDI sensitivity can be enhanced for certain classes of analytes by selectively modifying a combination of matrices, solvents, washing steps, rehydration of the matrix layer, as well as the matrix deposition method to selectively improve their desorption/ionization efficiencies over other analytes.[8−12] In the majority of cases, the matrix is applied over the tissue section by either spray deposition or sublimation.[13,14]

Pre-coated MALDI substrates have previously been reported and allow the user to prepare and characterize high-quality targets ahead of time while minimizing the number of steps for sample preparation.[15−17] While these pre-coated slides have yielded remarkable results, they are problematic for some studies.[15−17] To address the challenges associated with sample preparation for implementing pre-coated MALDI slides, there have been techniques developed that require minimal sample preparation.[18−20] Silicon nanopost arrays (NAPA) have shown potential as a matrix-free laser desorption ionization (LDI) substrate that enhances ionization of neutral lipid species while still maintaining some phospholipid signals.[21,22] Although NAPA has been shown to dramatically improve the signal of neutral lipids compared to traditional MALDI, the signal amplification of these species comes at the expense of certain phospholipid classes such as phosphatidylcholines (PCs) due to in-source fragmentation from the high laser energy requirement of NAPA for desorption/ionization to occur.[21,22] Recently, tissue sections thaw-mounted onto bare NAPA have been coated with 2,5-dihydrobenzoic acid (DHB)

Received: April 13, 2021
Accepted: August 16, 2021
Published: August 27, 2021

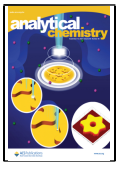






https://doi.org/10.1021/acs.analchem.1c01560
*Anal. Chem.* 2021, 93, 12243−12249

to minimize phospholipid fragmentation by initially imaging phospholipids at lower laser energy by MALDI, followed by high laser energy irradiation of the same pixels, whereby the laser energy is coupled into the underlying nanoposts for neutral lipid visualization.[23] This strategy enables visualization of phospholipids, followed by visualization of neutral lipids from a single tissue section.[23] Other surface-assisted laser desorption/ionization technologies have also been successfully used for IMS applications.[24−27]

To improve the molecular coverage and sensitivity of pre-coated MALDI IMS targets, we have developed a MALDI matrix and salt pre-coated NAPA substrate that allows simultaneous imaging of most classes of phospholipids and neutral lipids using a single polarity at high spatial resolution. Importantly, the pre-coated NAPA substrate requires no further sample preparation after thaw-mounting of the tissue section. This approach significantly reduces the laser fluence needed for efficient desorption/ionization, increases phospholipid signals, and enhances sensitivity for neutral lipids as compared to bare NAPA. To thoroughly investigate pre-coated NAPA substrates for MALDI IMS, sample optimization was conducted with various matrices and salts. These include α-cyano-4-hydroxycinnamic acid (CHCA), 2,5-dihydroxyacetophenone (DHA), 2,5-dihydrobenzoic acid (DHB), and 1,5-diaminonaphthalene (DAN) along with Li, Na, and K salts using various types of mimetic tissue homogenates with varying thicknesses. The experimentally determined optimal conditions were then applied to MALDI IMS experiments of mouse brain and rat retinal tissues, enabling the simultaneous visualization of phospholipids and neutral lipids from a matrix and salt pre-coated silicon nanofabricated substrate at high spatial resolution.

## MATERIALS AND METHODS

**Chemicals and Reagents.** Tri-potassium citrate monohydrate ($K_3Ci$), Tri-sodium citrate dihydrate ($Na_3Ci$), and tri-lithium citrate tetrahydrate ($Li_3Ci$) along with all high-performance liquid chromatography (HPLC) grade solvents were purchased from the Fisher Scientific Company (Suwanee, GA). 2,5-Dihydroxybenzoic acid, 2,5-dihydroxyacetophenone, α-cyano-4-hydroxycinnamic acid, 1,5-diaminonaphthalene, and red phosphorus were purchased from Sigma-Aldrich (St. Louis, MO). Indium-tin-oxide (ITO) microscope slides were purchased from Delta Technologies (Loveland, CO).

**NAPA Chips Nanofabrication.** Silicon nanoposts array fabrication followed a previously published procedure.[28] In short, low resistivity (0.001−0.005 Ω cm) p-type silicon wafers from Silicon Valley Microelectronics Inc. (Santa Clara, CA) were exposed to a deep ultraviolet projection photolithography process, followed by deep reactive etching. This process produced nanopost with dimensions of 1100 nm in height, 150 nm in diameter, and periodicity of 350 nm. After treatment, the wafers were cut into 20 mm squares for ease of use.

**Matrix and Salt Pre-Coating.** A solution composed of 5.5 mg/mL CHCA (∼30 mM) and 0.7 mg/mL tri-basic potassium citrate (∼7 mM potassium) in 8:2 MeOH/$H_2O$ was prepared. This matrix and salt solution was sprayed using a M3 TM-Sprayer from HTX Technologies (Chapel Hill, NC) for a final density of 0.41 μg/mm$^2$ (2.2 nM/mm$^2$) and 0.05 μg/mm$^2$ (∼0.5 nM/mm$^2$ of potassium), respectively. The specific method parameters for the TM-Sprayer can be found in Table S1. For the matrix comparison test, addition of the MALDI matrices followed their own respective protocol (Table S1).

**Tissue Sampling and Sectioning.** Frozen juvenile mouse brain and liver along with frozen juvenile rat eye were purchased from BioReclamation (Hicksville, NY). Juvenile rabbit adrenal gland and testis were purchased from Pel-Freez Biologicals (Rogers, AR). Tissue homogenates were prepared by following already published procedures.[29] In short, precut organs from 2 to 3 animals were homogenized using a 1.5 mL Navy Blue Bead Lysis Kit and a Stormy BBY24M bead beater Next Advance (Troy, NY). The homogenized solutions from multiple tubes of the same organ type were pooled. The pooled homogenates were placed into a cylindrical OCT mold and placed in a −80 °C freezer until use. Tissues were cut at 10 μm thickness using a CM3050S cryostat from Leica Microsystems (GmbH, Wetzlar, Germany) and thaw-mounted on various types of surfaces such as NAPA, pre-coated NAPA, or ITO slides. Tissues were then dried in a desiccator for 20 min prior to analysis or sample preparation. Serial sections were collected for hematoxylin and eosin (H&E) staining using an in-house protocol (Table S2).

**Scanning Electron Microscopy (SEM) Analysis.** Scanning electron microscopy images were acquired using a SEM Merlin from Carl Zeiss (White Plains, NY). NAPA chips with mounted tissues were mounted onto an ITO slide using double sided carbon tape and were coated with a 3.0 nm layer of sputtered gold (99.99% purity) using a Cressington 208HR sputter coater from de Ted Pella Inc. (Redding, CA) prior to SEM measurements. Spot sizes were determined by averaging 10 randomly selected on-tissue ablation spots in both their vertical and horizontal planes using the SEM Merlin measuring tool.

**LDI and MALDI Mass Spectrometry.** Profiling and IMS of the tissue sections were performed on a 9.4T or 15T solariX MALDI Fourier-transform ion cyclotron resonance (FT-ICR) mass spectrometer from Bruker Daltonics (Billerica, MA) in positive ion mode. Data acquisition was performed using FTMS control 2.2.0 in conjunction with flexImaging 5.0 (Bruker Daltonics, Billerica, MA). Instrument calibration was performed prior to MS and IMS analyses using red phosphorus. Post-process internal calibration was performed using five known signals found across the mass range. Lipid identification was carried out by comparing accurate mass measurement (≤1 ppm) with the LIPID MAPS[30] and/or the HMDB[31] databases along with MS/MS experiments using collision-induced dissociation (CID) on a 15T solariX MADLI FT-ICR MS (Bruker Daltonics, Billerica, MA) using a previously published method.[5] Imaging data spatial resolution is defined by the step size of the sample stage (pitch) and the diameter of the focused laser at the sample surface (spot size) and varied from 10 to 25 μm for FT-ICR IMS experiments. Positive ion mode IMS of rat eye tissue was performed on a prototype MALDI timsTOF Pro in Q-TOF mode at a spatial resolution of 10 μm.[32] More detailed information for the instrumental parameters can be found in Supporting Information and in Table S3.

**Data Analysis.** Data analysis was performed with DataAnalysis 5.0, ftmsProcessing 2.2.0, flexImaging 5.0, and SCiLS 5.00.9510 (Bruker Daltonics, Billerica, MA). Reported signal-to-noise ratios were calculated using DataAnalysis, ftmsProcessing, and/or mMass.[33] Using DataAnalysis, the intensity from the most abundant signals from each observable lipid class were summed together from the average spectra of a 20 × 20 pixel array IMS image performed on tissue homogenates (technical replicate: $n$ = 3). These summed signal intensities


https://doi.org/10.1021/acs.analchem.1c01560
Anal. Chem. 2021, 93, 12243−12249

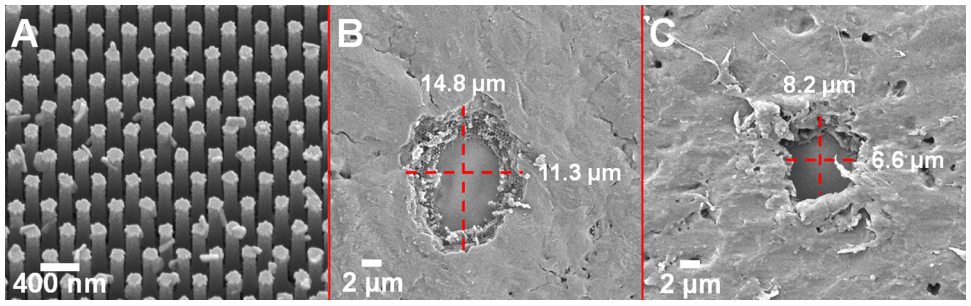


**Figure 1.** (A) SEM image of a NAPA substrate after addition of CHCA and potassium salts at 75 000× magnification with a 30° angle showing the nanoscale crystal of matrix and salt lying on the silicon nanopost. SEM images of tissues at a magnification of 5000× from a typical ablation crater with diameter of (B) 13 ± 2 $\mu$m and (C) 8 ± 1 $\mu$m after laser irradiation from prototype MALDI timsTOF Pro with a SmartBeam three-dimensional (3D) laser at 35 and 23% total laser power, respectively.

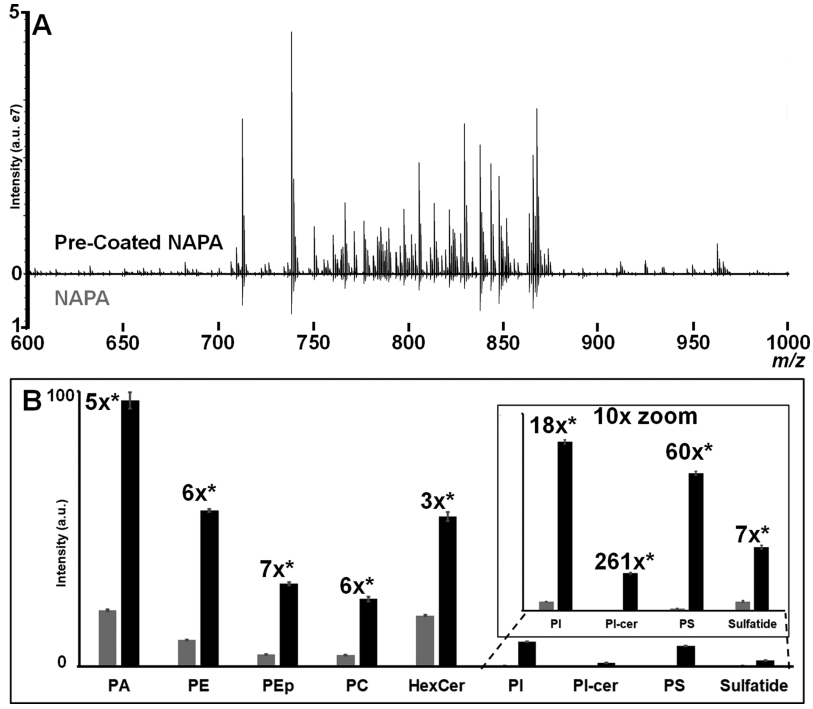


**Figure 2.** (A) Mass spectrum of pre-coated NAPA (top) and bare NAPA (bottom) scaled to the same intensity from one of their respective replicates. (B) Fold changes visualization between bare NAPA (gray) and pre-coated NAPA (black) for different classes of detected lipids ($n$ = 3). * $p$-value ≤ 0.05..

were then averaged for each lipid class for comparison of sample preparation conditions (See Supporting Information). This final lipid species-specific average was compared across all experimental conditions. Statistical significance between groups was computed using Student's $t$-test with a 95% confidence interval.

## RESULTS AND DISCUSSION

**Pre-Coated NAPA Optimization.** We present the use of a pre-coated NAPA chip with CHCA and potassium salts to enable the simultaneous visualization of both phospholipids and neutral lipids from biological tissue sections at high spatial resolution in a single IMS experiment. To determine the optimal conditions for pre-coating of NAPA chips, four commonly employed MALDI matrices (DAN, DHA, DHB, and CHCA) used primarily for targeting lipids were tested without the addition of salts. The results showed that both DHA and DAN failed to efficiently ionize HexCer in the brain homogenate and were no longer considered for further experimentation (Figure S1). In the cases of DHB and CHCA, both provided broad molecular coverage for all tissue types but were not observed to be significantly different (Figures S1 and S2). Due to its known nanometer-scale crystal size and vacuum stability, CHCA was selected for further optimization.[6] Previously published work on matrix and salt doping showed that multivalent salts reduced the amount of salt needed for proper ionization of neutral lipids that help maintain tissue integrity while minimizing adverse effects on the desorption/ionization process.[5] With this in mind, we proceeded to assess the effect of pre-coating NAPA with $Li_3Ci$, $Na_3Ci$, $K_3Ci$ at previously published levels with and without CHCA.[5] Pre-coating of salts on a NAPA chip without matrix yielded no significant changes in lipid signal compared to undoped NAPA, as previously observed.[21] All three salt doping experiments performed with CHCA pre-coating showed that potassium adducts were the predominant ion species, even in the presence of additional sodium or lithium salt (Figure S3). Additionally, it is noted that for both bare and pre-coated


https://doi.org/10.1021/acs.analchem.1c01560
Anal. Chem. 2021, 93, 12243−12249

NAPA, protonated species were not observed. We hypothesize that this is in part due to the high thermal energy requirement of the NAPA desorption process under Gaussian laser irradiation that favors potassium adduct formation compared to traditional MALDI, where sodium adduct formation is typically favored for neutral lipid ionization.[5,21,34] To optimize the amount of salt and matrix needed for pre-coated NAPA, both the amount of salt and matrix deposited were gradually reduced until the presence of matrix clusters was minimized and lipid signal intensity maximized.[5,34] A surface concentration of 0.41 $\mu$g/mm$^2$ (2.2 nM/mm$^2$) CHCA and 0.05 $\mu$g/mm$^2$ (~0.5 nM/mm$^2$) of tri-potassium citrate was found to both maximize lipid signal and minimize CHCA clusters in the mass spectrum.

We also explored the impact that pre-coated NAPA had on the required tissue thickness and necessary laser power for efficient desorption and ionization of lipids. Pre-coated NAPA chips were found to work with thicknesses $\leq$12 $\mu$m and at approximately two-thirds of the laser power typically required for bare NAPA.[21] This reduction in laser power resulted in smaller laser ablation spot sizes. Visualization of laser ablation craters from SEM analysis after IMS showed a reduction of ablation craters diameter from 13 $\pm$ 2 $\mu$m at regular NAPA laser power (35% total laser power) down to 8 $\pm$ 1 $\mu$m with the pre-coated NAPA lower laser power (23% total laser power) using the MALDI timsTOF platform (Figure 1). While this reduction in laser power leads to a significant drop in signal intensity from bare NAPA, the pre-coated NAPA chip maintained both high signal intensity and signal to noise for the detected lipids (Figure 2 and Table S4). With the combination of CHCA and potassium salts as pre-coating agents for NAPA, we obtained at least a ~5.8 $\pm$ 0.1-fold increase in phospholipid and at least a ~2.0 $\pm$ 0.1-fold increase in neutral lipid signal compared to bare NAPA, depending on lipid species and tissue type at identical laser power ($n$ = 3) (Figures 2 and S4). Looking into the phospholipid fold change experiment data more carefully, three trends were observed. First, phospholipids that bare NAPA can easily ionize such as phosphatidic acids (PAs), phosphatidylethanolamines (PE), and their plasmalogen counterparts (PEp) showed an intensity fold change of about one order of magnitude with pre-coated NAPA. Second, lipids that are typically either not detected or detected with low intensity using bare NAPA such as phosphatidylinositols (PI), PI ceramides (PI-Cer), phosphatidylserines (PS), and sulfatides showed an increase in sensitivity of 1−2 orders of magnitude. Pre-coated NAPA enabled high-quality ion images to be generated for these species, whereas with bare NAPA, most images were too noisy to distinguish the localization of these species properly (Figure S5). Finally, pre-coated NAPA improved PC sensitivity (5-fold to an order of magnitude), likely due to a combination of higher ionization efficiency and a reduction in in-source fragmentation of the head group, leading to PA-like fragment ions, as observed with bare NAPA.[35] These global increases in lipid signals can partially be explained through enhancement of the ionization efficiency of desorbed analytes from pre-coated NAPA by the addition of both matrix and salt, particularly for phospholipid analytes. Further investigation of this new MALDI pre-coated substrate using MALDI-2 was explored. However, no changes were observed in the mass spectrum upon MALDI-2 activation (data not shown).

**Comparing the Image Quality of NAPA and Pre-Coated NAPA Samples.** Serial mouse brain tissue sections were imaged at a 25 $\mu$m spatial resolution on a 9.4T MALDI FT-ICR mass spectrometer using both bare NAPA and pre-coated NAPA as substrate. Instrumental settings were optimized for high spatial resolution imaging (e.g., reduced laser power). Mouse brain tissue sections serve as an ideal candidate for high spatial resolution IMS experiments due to their various small histological features, as well the wide variety of phospholipids and cerebrosides. Figure 3 shows both NAPA and pre-coated NAPA lipid ion images, scaled at the same intensities for each ion, illustrating the enhancement in lipid signal for pre-coated NAPA substrates. Additionally, pre-coated NAPA promotes the ionization of PIs and PSs, lipid classes that are not typically observed in positive ion mode analysis using bare NAPA (Figure S5). This leads to better visualization of many signals such as HexCer (32:1;O2) that correlates to the gray matter of the brain along with PS (40:6). Other cerebrosides, such as HexCer(40:1;O3), correlate to the white matter of the brain as structural components of the myelin sheet (Figure 3).[36] PE (38:4) and PI (38:4) both have

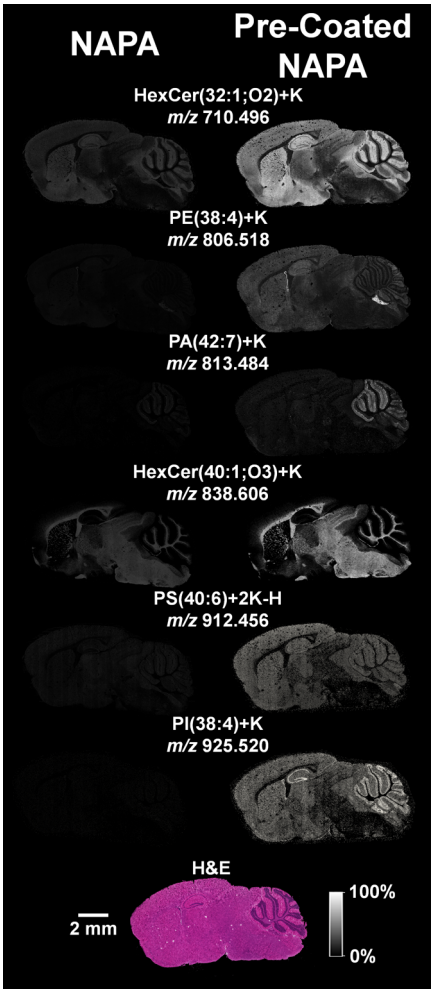


**Figure 3.** LDI and MALDI IMS of a sagittal mouse brain tissue section thaw-mounted on either NAPA or pre-coated NAPA substrate. IMS was acquired using a 9.4T FT-ICR mass spectrometer with a spatial resolution of 25 $\mu$m at identical laser power and number of laser shots. Intensities of both NAPA and pre-coated NAPA ion images were normalized to one another. In all instances, the pre-coated NAPA substrate outperformed NAPA for all detected lipid classes.


https://doi.org/10.1021/acs.analchem.1c01560
Anal. Chem. 2021, 93, 12243−12249

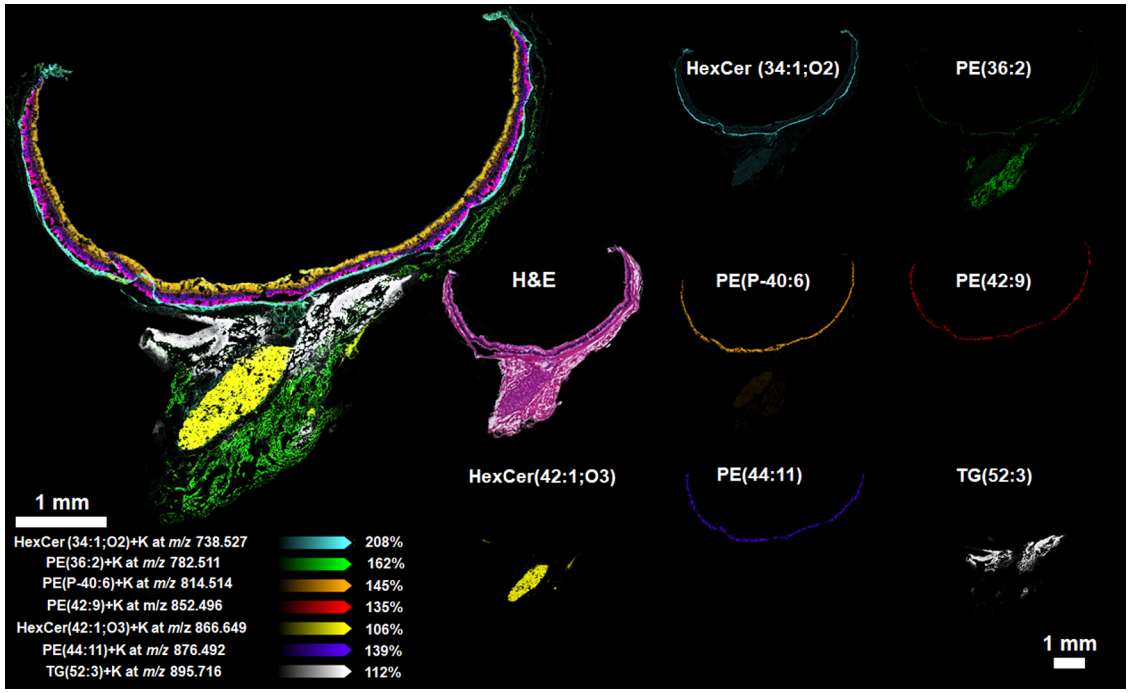


**Figure 4.** MALDI IMS of an albino rat eye tissue section with a lateral resolution of 10 $\mu$m using a prototype MALDI timsTOF Pro in positive ion mode. Pre-coated NAPA substrate allows the simultaneous detection of various lipids such as cerebrosides, phosphatidylethanolamines, and triacylglycerols at high spatial resolution.

very distinct ion images, one correlating to both the lateral ventricle along with the lateral recess and the second with the granular cell layer of both the hippocampus and the cerebellum, respectively. Finally, PA (42:7) that is most likely the product of in-source fragmentation can be found in the gray matter of the cerebellum with higher intensity at the interface between the molecular layer and the granular layer, where Purkinje cells are found. The improved sensitivity that matrix/salt pre-coated NAPA affords for a broad range of lipid classes improves both image contrast and the achievable IMS image resolution, enabling a more complete description of in situ lipidomic features within the tissue microenvironment.

**Pre-Coated NAPA for High Spatial Resolution MALDI IMS.** To assess the utility of matrix/salt pre-coated NAPA targets for high spatial resolution IMS, 10 $\mu$m lateral resolution images of albino rat retinal tissue were generated using a MALDI timsTOF mass spectrometer. Ion images of various lipids from an albino rat retina acquired at 10 $\mu$m lateral resolution can be found in Figures 4 and S6. At high spatial resolution, it was possible to visualize eight of the nine different cell layers that comprise the retina through the ionization of multiple lipid species, each having distinct spatial distributions. We were also able to detect the species associated with the optic nerve, where most HexCer lipids were found to localize, including HexCer (42:1;O3). One notable exception was HexCer (34:1;O2) that was found primarily in the photoreceptor layer and the retinal pigment layer. Phosphatidylethanolamines were found to have a more widespread distribution with PE (40:6) being detected in the outer nuclear layer, PE (44:11) being detected in the three central layers (outer nuclear layer, outer plexiform layer, and inner nuclear layer), and PE (P-40:6) localizing to the three inner retina layers (inner plexiform layer, ganglion cell layer, and nerve fiber layer) (Figure S7).

## CONCLUSIONS

With the increasing use of MALDI IMS, there is a need for extremely simple, unambiguous sample preparation strategies that provide broad molecular coverage from a single experiment, high sensitivity capabilities, and potential for high throughput data acquisition. This work shows that pre-coating NAPA with ~0.41 $\mu$g/mm$^2$ of CHCA and ~0.05 $\mu$g/mm$^2$ of $K_3Ci$ both enhanced molecular coverage of lipid classes and increased sensitivity when compared to bare NAPA. In addition, matrix/salt pre-coated NAPA requires no further sample preparation beyond cryo-sectioning of the tissue, minimizing possible sample degradation due to lengthy sample preparation.[37,38] We have demonstrated the enhanced sensitivity of this approach by performing high spatial resolution IMS using a matrix pre-coated nanofabricated substrate. The potential to monitor the distribution and composition of both polar and neutral lipids simultaneously with minimal sample preparation at high spatial resolution will allow for a more rapid and thorough study of biological systems where lipid metabolism is a critical factor in the associated biology.

## ASSOCIATED CONTENT

### Supporting Information

The Supporting Information is available free of charge at https://pubs.acs.org/doi/10.1021/acs.analchem.1c01560.

Instrumental parameters, method details, M5 sprayer parameters (Table S1), H&E staining protocol (Table S2), instrumental parameters (Table S3), intensity vs S/N comparisons (Table S4), average spectra from rabbit adrenal gland and mouse brain homogenates (Figure S1), average spectra from mouse liver and rat testis homogenates (Figure S2), average spectra comparing pre-coating using different alkali metal salts (Figure S3),



https://doi.org/10.1021/acs.analchem.1c01560
Anal. Chem. 2021, 93, 12243−12249

fold change data from tissue homogenates (Figure S4), mouse brain ion images (Figure S5), individual ion images from albino rat eye tissue using pre-coated NAPA (Figure S6), and H&E stained tissue from albino rat eye (Figure S7) (PDF)

Raw ion intensities used to calculate reported fold changes can be found in the provided spreadsheet (XLSX)

## AUTHOR INFORMATION


### Corresponding Author

**Jeffrey M. Spraggins** − *Mass Spectrometry Research Center and Department of Chemistry, Vanderbilt University, Nashville, Tennessee 37235, United States; Department of Biochemistry, Vanderbilt University, Nashville, Tennessee 37205, United States; Department of Cell & Developmental Biology, Vanderbilt University, Nashville, Tennessee 37232, United States;* orcid.org/0000-0001-9198-5498; Email: jeff.spraggins@vanderbilt.edu

### Authors

**Martin Dufresne** − *Mass Spectrometry Research Center, Vanderbilt University, Nashville, Tennessee 37235, United States; Department of Biochemistry, Vanderbilt University, Nashville, Tennessee 37205, United States*

**Jarod A. Fincher** − *Mass Spectrometry Research Center, Vanderbilt University, Nashville, Tennessee 37235, United States; Department of Biochemistry, Vanderbilt University, Nashville, Tennessee 37205, United States*

**Nathan Heath Patterson** − *Mass Spectrometry Research Center, Vanderbilt University, Nashville, Tennessee 37235, United States; Department of Biochemistry, Vanderbilt University, Nashville, Tennessee 37205, United States;* orcid.org/0000-0002-0064-1583

**Kevin L. Schey** − *Mass Spectrometry Research Center and Department of Chemistry, Vanderbilt University, Nashville, Tennessee 37235, United States; Department of Biochemistry, Vanderbilt University, Nashville, Tennessee 37205, United States*

**Jeremy L. Norris** − *Mass Spectrometry Research Center and Department of Chemistry, Vanderbilt University, Nashville, Tennessee 37235, United States; Department of Biochemistry, Vanderbilt University, Nashville, Tennessee 37205, United States*

**Richard M. Caprioli** − *Mass Spectrometry Research Center and Department of Chemistry, Vanderbilt University, Nashville, Tennessee 37235, United States; Department of Biochemistry, Vanderbilt University, Nashville, Tennessee 37205, United States; Department of Pharmacology, Vanderbilt University, Nashville, Tennessee 37232, United States*

Complete contact information is available at: https://pubs.acs.org/10.1021/acs.analchem.1c01560


### Notes

The authors declare no competing financial interest.

## ACKNOWLEDGMENTS

Scanning electron microscopy measurements were performed at the Vanderbilt Institute of Nanoscale Science and Engineering. Support for these studies was provided by the National Institutes of Health (NIH) National Institute of General Medical Sciences (P41 GM103391 awarded to R.M.C.) and the NIH Common Fund and National Eye Institute (U54EY032442 awarded to J.M.S., K.L.S., and R.M.C.). The prototype MALDI timsTOF MS was developed as part of the National Science Foundation Major Research Instrument Program (CBET—1828299 awarded to J.M.S. and R.M.C.) and the Bruker 15T solariX FT-ICR MS in the Mass Spectrometry Research Center at Vanderbilt University was acquired through the NIH Shared Instrumentation Grant Program (1S10OD012359 awarded to R.M.C.).

## REFERENCES


(1) Caprioli, R. M.; Farmer, T. B.; Gile, J. *Anal. Chem.* **1997**, *69*, 4751−4760.
(2) Buchberger, A. R.; DeLaney, K.; Johnson, J.; Li, L. *Anal. Chem.* **2018**, *90*, 240−265.
(3) Spraker, J. E.; Luu, G. T.; Sanchez, L. M. *Nat. Prod. Rep.* **2020**, *37*, 150−162.
(4) Lauzon, N.; Dufresne, M.; Chauhan, V.; Chaurand, P. *J. Am. Soc. Mass Spectrom.* **2015**, *26*, 878−886.
(5) Dufresne, M.; Patterson, N. H.; Norris, J. L.; Caprioli, R. M. *Anal. Chem.* **2019**, *91*, 12928−12934.
(6) Niehaus, M.; Soltwisch, J.; Belov, M. E.; Dreisewerd, K. *Nat. Methods* **2019**, *16*, 925−931.
(7) Aichler, M.; Walch, A. *Lab. Invest.* **2015**, *95*, 422−431.
(8) Yang, J.; Caprioli, R. M. *Anal. Chem.* **2011**, *83*, 5728−5734.
(9) Yang, E.; Dufresne, M.; Chaurand, P. *Int. J. Mass Spectrom.* **2017**, *437*, 3−9.
(10) Seeley, E. H.; Oppenheimer, S. R.; Mi, D.; Chaurand, P.; Caprioli, R. M. *J. Am. Soc. Mass Spectrom.* **2008**, *19*, 1069−1077.
(11) Angel, P. M.; Spraggins, J. M.; Baldwin, H. S.; Caprioli, R. *Anal. Chem.* **2012**, *84*, 1557−1564.
(12) Thomas, A.; Charbonneau, J. L.; Fournaise, E.; Chaurand, P. *Anal. Chem.* **2012**, *84*, 2048−2054.
(13) Hankin, J. A.; Barkley, R. M.; Murphy, R. C. *J. Am. Soc. Mass Spectrom.* **2007**, *18*, 1646−1652.
(14) Stoeckli, M.; Chaurand, P.; Hallahan, D. E.; Caprioli, R. M. *Nat. Med.* **2001**, *7*, 493−496.
(15) Grove, K. J.; Frappier, S. L.; Caprioli, R. M. *J. Am. Soc. Mass Spectrom.* **2011**, *22*, 192−195.
(16) Yang, J.; Caprioli, R. M. *Anal. Chem.* **2013**, *85*, 2907−2912.
(17) Yang, J.; Caprioli, R. M. *Anal. Chem.* **2013**, *85*, 2907−2912.
(18) Takáts, Z.; Wiseman, J. M.; Gologan, B.; Cooks, R. G. *Science* **2004**, *306*, 471−473.
(19) Nemes, P.; Vertes, A. *Anal. Chem.* **2007**, *79*, 8098−8106.
(20) Castaing, R.; Slodzian, G. *C. R. Hebd. Seances Acad. Sci.* **1962**, *255*, No. 1893.
(21) Fincher, J. A.; et al. *J. Comput. Neurol.* **2019**, *527*, 2101−2121.
(22) Fincher, J. A.; et al. *Sci. Rep.* **2019**, *9*, No. 17508.
(23) Fincher, J. A.; Korte, A. R.; Yadavilli, S.; Morris, N. J.; Vertes, A. *Analyst* **2020**, *145*, 6910−6918.
(24) Patti, G. J.; et al. *Neuroscience* **2010**, *170*, 858−864.
(25) Picca, R. A.; Calvano, C. D.; Cioffi, N.; Palmisano, F. *Nanomaterials* **2017**, *7*, No. 75.
(26) Nizioł, J.; Rode, W.; Laskowska, B.; Ruman, T. *Anal. Chem.* **2013**, *85*, 1926−1931.
(27) Palermo, A.; et al. *ACS Nano* **2018**, *12*, 6938−6948.
(28) Morris, N. J.; et al. *RSC Adv.* **2015**, *5*, 72051−72057.
(29) Groseclose, M. R.; Castellino, S. *Anal. Chem.* **2013**, *85*, 10099−10106.
(30) Sud, M.; et al. *Nucleic Acids Res.* **2007**, *35*, D527−D532.
(31) Wishart, D. S.; et al. *Nucleic Acids Res.* **2018**, *46*, D608−D617.
(32) Spraggins, J. M.; et al. *Anal. Chem.* **2019**, *91*, 14552−14560.
(33) Strohalm, M.; Hassman, M.; Košata, B.; Kodíček, M. *Rapid Commun. Mass Spectrom.* **2008**, *22*, 905−908.
(34) Dufresne, M.; Masson, J. F.; Chaurand, P. *Anal. Chem.* **2016**, *88*, 6018−6025.
(35) Fincher, J. A.; et al. *J. Mass Spectrom.* **2020**, *55*, No. e4443.

(36) Jurevics, H.; et al. *J. Neurochem.* **2001**, *77*, 1067−1076.
(37) Patterson, N. H.; Thomas, A.; Chaurand, P. *J. Mass Spectrom.* **2014**, *49*, 622−627.
(38) Lukowski, J. K.; et al. *J. Am. Soc. Mass Spectrom.* **2020**, *31*, 2538−2546.



https://doi.org/10.1021/acs.analchem.1c01560
*Anal. Chem.* 2021, 93, 12243−12249